

Magnetoelastic signatures of conical state and charge density waves in antiferromagnetic FeGe

L. Prodan,^{1,*} J. Sourd,² and L. Chioncel^{3,4}

¹*Experimentalphysik V, Center for Electronic Correlations and Magnetism, Institute of Physics, University of Augsburg, D-86159 Augsburg, Germany*

²*Hochfeld-Magnetlabor Dresden (HLD-EMFL) and Würzburg-Dresden Cluster of Excellence ct.qmat, Helmholtz-Zentrum Dresden-Rossendorf, 01328 Dresden, Germany*

³*Theoretische Physik III, Institute of Physics, University of Augsburg, D-86135 Augsburg, Germany*

⁴*Augsburg Center for Innovative Technologies, University of Augsburg, 86135 Augsburg, Germany*

We present a unified magnetoelastic framework describing ultrasound velocity anomalies in antiferromagnetic FeGe under low magnetic fields applied along the c axis. A global multi-field analysis reveals the pronounced low-temperature anomaly near 35 K originates from hybridization between longitudinal acoustic phonons and a field-dependent magnetic mode associated with the exchange-driven conical spin structure, while the shoulder near 100 K arises from a field-independent charge density wave (CDW) susceptibility channel. The fitted parameters exhibit strong internal scaling relations, allowing the data to collapse onto universal magnetic and CDW scaling curves. By explicitly connecting the magnetic scaling variable to the cone angle measured by neutron diffraction, we establish a quantitative link between ultrasound softening and the evolution of the transverse spiral component of the double-cone structure. Our results therefore unify elastic and neutron-scattering observations within a single phenomenological framework and demonstrate that $\Delta v/v$ provides a sensitive probe of coupled magnetic and electronic instabilities in FeGe.

Introduction. The B35-type FeGe has recently emerged as an intriguing platform for investigating how magnetic, electronic, and lattice degrees of freedom couple to produce emergent phenomena. The compound develops A-type antiferromagnetic (AFM) order below $T_N \approx 410$ K, consisting of ferromagnetically aligned Fe moments within the kagome planes that are AFM coupled along the c axis, Fig. 1(a) [1, 2]. The discovery of charge-density-wave (CDW) state below $T_{CDW} \approx 110$ K [3], has stimulated extensive experimental and theoretical efforts. Detailed investigations using x-ray and neutron diffraction [3–7], angle-resolved photoemission [8], Raman spectroscopy [9], and scanning tunneling microscopy [10], supported by theoretical calculations [11–13], have revealed that partial dimerization of Ge atoms along the c axis gives rise to a $2 \times 2 \times 2$ crystallographic superstructure. This structural modulation stabilizes the CDW order with a multiple propagation vector \mathbf{q} deep inside the AFM state and it is accompanied by an enhancement of the ordered magnetic moments below T_{CDW} [3, 6, 8, 14].

Below $T \approx 60$ K, the magnetic state of FeGe evolves into a spin-canted phase in which the Fe moments progressively tilt away from the c axis toward the kagome plane, forming a double-cone-like spin configuration with a finite in-plane component, Fig. 1(a) and (b) [2, 15]. In this regime, neutron diffraction and inelastic neutron scattering measurements further suggest the emergence of incommensurate magnetic correlations characterized by a modulation of the magnetic order along the c axis [5, 16, 17]. Taken together, these neutron diffraction

and spectroscopy results demonstrate that the magnetic, charge, and lattice degrees of freedom become strongly intertwined below ~ 100 K [18]. Such low-energy spin, charge, and orbital fluctuations contribute to the corresponding electronic susceptibilities, which renormalize the elastic constants of the material and thereby influence the propagation of acoustic waves [19, 20]. The velocity of an acoustic mode is given by $v = \sqrt{C/\rho}$, where C denotes the elastic constant and ρ the material density. Consequently, sound velocity measurements provide direct access to fluctuation-induced changes in the elastic response. In metallic antiferromagnets, both magnons and low-energy spin fluctuations couple to strain via exchange-striction and magnetic anisotropy mechanisms, making the elastic constants sensitive to magnetic correlations [21, 22]. Ultrasound experiments therefore offer a powerful probe of the interplay between spin, charge, and lattice degrees of freedom across competing ordered phases [20, 21, 23].

Here, we employ ultrasound propagation measurements to probe spin-charge-lattice coupling in noncollinear antiferromagnet FeGe. The relative change in the longitudinal sound velocity, $\Delta v/v$, exhibits pronounced anomalies near ~ 100 K and ~ 35 K, corresponding to the onset of the CDW phase and the low-temperature conical magnetic state, respectively. Upon applying a magnetic field along the c axis, we find that the anomaly at T_{CDW} is nearly field independent, whereas the lower-temperature anomaly evolves strongly with increasing field. To describe these observations, we develop a multi-mode model that treats phonons, magnons, and CDW amplitude as coupled quantum fields and evaluates their interactions within the Green's function formalism. The resulting fitting expression quantitatively captures both anomalies in the sound velocity, including

* Corresponding author: lilian.prodan@uni-a.de

their distinct field dependence. We demonstrate that the low-temperature anomaly near 35 K originates from hybridization between longitudinal acoustic phonons and a field-dependent magnetic excitation, while the anomaly at T_{CDW} arises from a separate electronic susceptibility channel associated with the CDW instability.

Experimental details. Polycrystalline FeGe was synthesized from high-purity elemental precursors using a conventional solid-state reaction method. Single crystals were subsequently grown by chemical vapor transport using the polycrystalline precursor as the starting material. Crystal growth was performed in a two-zone horizontal furnace with a temperature gradient of $\sim 520^\circ\text{C} - 480^\circ\text{C}$, employing iodine as the transport agent. Phase purity, chemical composition, and sample homogeneity were verified by energy-dispersive X-ray spectroscopy (EDS) using a ZEISS Crossbeam 550 system. Magnetic properties were measured using a SQUID magnetometer (Quantum Design MPMS 3) in the temperature range 2–400 K under magnetic fields up to 7 T, applied both parallel and perpendicular to the crystallographic c axis.

The ultrasound measurements were performed utilizing the transmission pulse-echo technique with phase sensitive detection [19, 21]. For the longitudinal elastic modes both the propagation vector k and polarization u were applied along the c axis. A frequency of 40 MHz was used together with LiNbO₃ transducers. The experiments were performed in static magnetic fields using the Quantum Design PPMS system.

Static (dc) magnetic susceptibility, χ , of single-crystalline FeGe was measured with the magnetic field applied both parallel and perpendicular to the crystallographic c axis. Figure 1(c) displays the temperature dependence of χ measured after zero-field cooling in an applied magnetic field of 1 T. For $H \parallel c$, a gradual change is observed at about 400 K, consistent with the approach to the Néel temperature $T_N \approx 410$ K. Upon cooling, $\chi(T)$ for $H \parallel a$ exhibits a pronounced anomaly below ~ 100 K, which has been associated with the onset of charge-density-wave (CDW) order [3]. No clear anomaly is resolved in $\chi(T)$ at the reported canting temperature $T \approx 60$ K, suggesting that this transition primarily modifies the spin configuration without significantly affecting magnetic response. At lower temperatures, around ~ 30 K, an upturn in χ is observed for $H \parallel c$, accompanied by a maximum in $\chi(T)$ for $H \parallel a$. At approximately the same temperature, neutron diffraction measurements reveal a maximum in the magnetic Bragg peak intensity, indicative of the cone half-angle [2].

Figure 2 reveals the experimentally measured relative change in sound velocity, $\Delta v/v$, for longitudinal acoustic waves propagating along the c axis. In zero magnetic field, $\Delta v/v$ exhibits a pronounced low-temperature anomaly near ~ 35 K and a broader shoulder around ~ 100 K. These features occur at temperatures comparable to those associated with the onset of the canted conical magnetic state and the formation of the CDW phase, as inferred from magnetic susceptibility and neu-

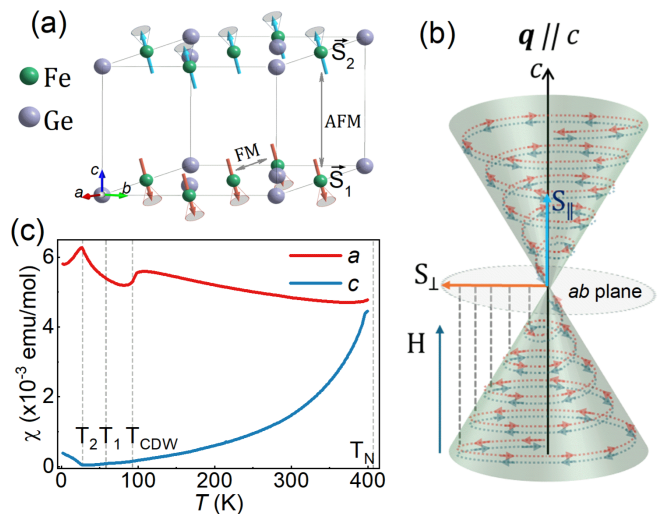


FIG. 1. (a) The hexagonal $P6/mmm$ crystal structure of FeGe. Canted arrows illustrate the low-temperature magnetic moment orientations with in-plane ferromagnetic (FM) and antiferromagnetic (AFM) ordering along the c axis. Transparent cones indicate the opening angle of the conical spin structure. (b) Schematic illustration of the low-temperature double-cone-structure with helical propagation vector $\mathbf{q} \parallel c$ and the field-modulated AFM double-cone state. Dashed vertical lines indicate the field-induced change of the in-plane projection of the ordered moment (cone angle) (i.e., the cone angle) for $H \parallel c$. (c) Temperature dependence of the zero-field cooled magnetic susceptibility χ measured in 1 T for $H \parallel a$ and c .

tron diffraction measurements, see Fig. 1(b) [3, 15]. Upon applying a magnetic field along the c axis, the minimum associated with the conical state shifts to higher temperatures, reaching approximately 45 K at 5 T. The amplitude of the relative change $\Delta v/v$ decreases with increasing field, indicating a field-induced modification of the longitudinal acoustic mode. In contrast, the anomaly at T_{CDW} remains nearly field independent.

Theoretical modeling. A general theoretical framework for multi-mode coupling has been put forward earlier in the context of superconductivity [24]. Assuming the weak coupling approach when phonons couple to magnons and CDW fluctuations, the phonon propagator becomes renormalized. The physical phonon frequencies follow from the poles of the dressed propagator. For the acoustic dispersion $\omega_{\mathbf{q}} = vq$, assuming weak coupling, $\omega_{\mathbf{q}} \approx \omega_{\mathbf{q}}^{(0)} + \delta\omega_{\mathbf{q}}$, and expanding to leading order yields the relative velocity change (see Appendix A):

$$\frac{\Delta v}{v} = \frac{\Re \Pi^{\text{ph}}(\mathbf{q}, \omega_{\mathbf{q}}^{(0)})}{2(\omega_{\mathbf{q}}^{(0)})^2} = \frac{1}{2C_0} \Re \Pi^{\text{ph}}(\mathbf{q} \rightarrow 0, \omega \rightarrow 0), \quad (1)$$

where $C_0 = \rho v_0^2$ is the bare elastic constant. In the long-wavelength limit ($\mathbf{q} \rightarrow 0$) ultrasound probes the quasi-static elastic response. The imaginary part of the self-energy governs sound absorption, $\alpha \propto \Im \Pi^{\text{ph}}(\mathbf{q}, \omega_{\mathbf{q}}^{(0)})/2\omega_{\mathbf{q}}^{(0)}$. Thus, all microscopic information

enters through the renormalized phonon self-energy Π^{ph} . Within perturbation theory the phonon self-energy can be expressed through collective susceptibilities [25], formally to be written as:

$$\Pi^{\text{ph}}(\mathbf{q}, \omega) = g_m^2 \chi_m(\mathbf{q}, \omega) + g_c^2 \chi_c(\mathbf{q}, \omega), \quad (2)$$

where g_m and g_c denote bilinear coupling constants between strain and the magnetic or CDW order-parameter fluctuations, respectively. This result can be also derived as Gaussian integration over the auxiliary fields and represents the leading-order self-energy correction generated by bilinear strain-order-parameter coupling (see Appendix B). In the long-wavelength limit, the relative sound-velocity change is therefore determined by the real part of the static self-energy, Eq. (1). In the following, rather than pursuing a fully microscopic evaluation, we introduce phenomenological forms of the susceptibilities suitable for describing the experimental data.

Susceptibility can be computed using standard many-body procedures [26]: one first evaluates the Matsubara polarization bubbles, then computes the interacting susceptibilities within the random-phase approximation and finally obtains the phonon self-energy. Well-known forms for the resulting effective susceptibilities for the CDW and (transverse) magnetic channels are (see Appendix C):

$$\chi_m^{\text{RPA}}(q, i\Omega_n) \propto \frac{1}{\Omega_n^2 + \omega^2(q, H, T) + \Gamma|\Omega_n|}, \quad (3)$$

$$\chi_c^{\text{RPA}}(q, i\Omega_n) \propto \frac{1}{a_c(T) + c_c(q - Q)^2 + \Gamma_c|\Omega_n|}. \quad (4)$$

These expressions provide a natural starting point for constructing phenomenological fitting forms for the sound-velocity renormalization. According to Eq. (1), the relevant quantity is the real part of the phonon self-energy taken in the limit $q \rightarrow 0$ and $\Omega_n \rightarrow 0$. Since the order of limits may not commute, one should first take the long-wavelength limit $q \rightarrow 0$ along the acoustic branch ($\omega \sim vq$) before sending $\Omega_n \rightarrow 0$, corresponding to the experimental ultrasound condition. Formally, the resulting static self-energy can be written as

$$\begin{aligned} \Pi^{\text{ph}}(0, 0) &= g_m^2 \frac{1}{\omega_0^2(T) + \alpha H^2 + \Gamma^2} \\ &+ g_c^2 \frac{1}{a_c(T - T_{\text{CDW}})^2 + \Gamma_c^2}. \end{aligned} \quad (5)$$

The magnetic contribution corresponds to a damped resonance originating from hybridization between acoustic phonons and transverse spin-wave modes. The CDW channel near a second-order instability, yielding a Lorentzian-like temperature dependence. The relative sound-velocity change is therefore governed by the real part of the fluctuation-induced phonon self-energy, providing a direct microscopic motivation for the phenomenological fitting expressions used below. According

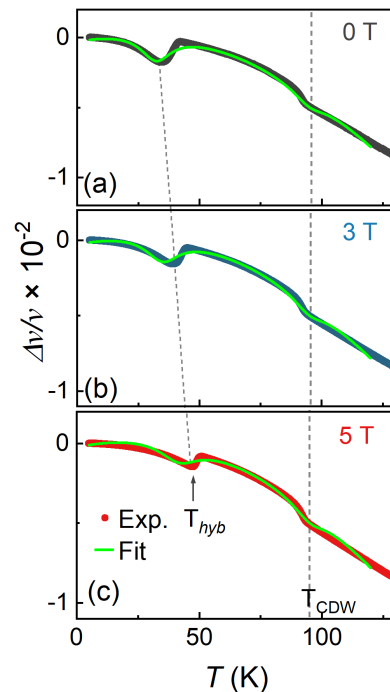


FIG. 2. Temperature dependence of the relative sound-velocity change, $\Delta v/v$, measured at magnetic fields of 0, 3, and 5 T. Data were obtained for the longitudinal acoustic mode with $\mathbf{k} \parallel c$ and $\mathbf{u} \parallel c$, with the magnetic field applied along the c axis. Dashed vertical lines mark the CDW transition temperature (T_{CDW}) and the hybridization temperature (T_{Hyb}), associated with the evolution of the magnetic cone half-angle. The green line corresponds to the fit using Eq. 11.

to Eq. (1), the relative sound-velocity change can be decomposed into contributions from a smooth lattice background, magnetic fluctuations, and CDW fluctuations,

$$\frac{\Delta v}{v} = \left(\frac{\Delta v}{v} \right)_{\text{bg}} + \left(\frac{\Delta v}{v} \right)_{\text{mag}} + \left(\frac{\Delta v}{v} \right)_{\text{CDW}}. \quad (6)$$

In addition to fluctuation-induced effects, the sound velocity exhibits a smooth temperature dependence arising from lattice anharmonicity and thermal expansion modeled phenomenologically as:

$$\left(\frac{\Delta v}{v} \right)_{\text{bg}} = a_0 + a_1 T + a_2 T^2, \quad (7)$$

where a_0 denotes the zero-temperature reference, a_1 accounts for linear thermal expansion, and a_2 captures the leading anharmonic contribution.

Following a similar algebraic form of the magnetic susceptibility within the static limit of eq. (3) we model the magnetic contribution as a damped resonance,

$$\chi_m(T, H) \propto \frac{1}{[a_m(T, H) - \omega_0]^2 + \Gamma^2(H)}, \quad (8)$$

where ω_0 denotes the acoustic mode energy scale entering the hybridization condition, and $\Gamma(H)$ is the mag-

netic damping. The effective magnetic stiffness is parameterized as $a_m(T, H) = a_{m0} + bT + \alpha H^2$, and the field-dependent damping as $\Gamma(H) = \Gamma_0 + \gamma H^2$. Physically, $a_m(T, H)$ represents the renormalized magnetic stiffness controlling the proximity to a magnetoelastic resonance with the acoustic branch. The quadratic field dependence is the lowest-order symmetry-allowed form in a centrosymmetric system; a negative α corresponds to field-induced softening of the relevant magnetic mode. At the denominator of $\chi_m(T, H)$ one can clearly see a possible redundancy of the model as a_{m0}, ω_0 and Γ_0 linearly dependent. We re-define $\delta_0 = a_{m0} - \omega_0$ as ω_0 is absorbed in a_{m0} , thus the magnetic contribution reads:

$$\left(\frac{\Delta v}{v}\right)_{\text{mag}} = -\frac{G_m}{[\delta_0 + bT + \alpha H^2]^2 + (\Gamma_0 + \gamma H^2)^2}. \quad (9)$$

with G_m is the effective magnetoelastic coupling strength.

Near a continuous CDW transition, Gaussian critical fluctuations yield an Ornstein–Zernike form which reduces to a Lorentzian-like susceptibility in the static limit which is similar to the form seen in eq. (4):

$$\left(\frac{\Delta v}{v}\right)_{\text{CDW}} = -\frac{G_c}{a_c(T - T_{\text{CDW}})^2 + \Gamma_c^2}. \quad (10)$$

Here G_c is the CDW–elastic coupling strength and Γ_c is the damping rate of the soft electronic mode approaching the CDW transition. The absence of a significant field dependence of this term in the fit supports its predominantly electronic origin and distinguishes it from the magnetically driven low-temperature anomaly. We observe that both a_c and Γ_c control the width of the velocity shift eq. (10), and thus, one can absorb a_c in the redefinition of Γ_c , i.e. in the fitting procedure we can fix $a_c = 1$ and fit only Γ_c . The full fitting function used for the global multi-field analysis is:

$$\begin{aligned} \frac{\Delta v}{v}(T, H) = & a_0 + a_1 T + a_2 T^2 \\ & - \frac{G_m}{[\delta_0 + bT + \alpha H^2]^2 + (\Gamma_0 + \gamma H^2)^2} \\ & - \frac{G_c}{(T - T_{\text{CDW}})^2 + \Gamma_c^2}. \end{aligned} \quad (11)$$

The simultaneous description of three magnetic fields, $H = 0, 3, 5$ T, with a single parameter set (see Tab. I) demonstrates that the decomposition into magnetic and CDW channels is internally consistent.

Figure 2 shows that the global fit captures the pronounced low-temperature anomaly near 35 K, its suppression and evolution with magnetic field, and the nearly field-independent CDW shoulder around 100 K. The minimum in the sound velocity occurs when the characteristic magnetic energy scale becomes comparable to the acoustic energy scale, $a_m(T, H) = \omega_0$, which yields the field-dependent dip position $T_{\text{dip}}(H) = (\omega_0 -$

TABLE I. Fit results with $\Gamma_0 \approx 5.29$ fixed, with values and uncertainties separated

Channel	param.	Value	Error
Background	a_0	-0.1937×10^{-3}	4.0812×10^{-6}
	a_1	3.7233×10^{-5}	1.7873×10^{-7}
	a_2	-8.3053×10^{-7}	2.0109×10^{-9}
Magnetic	δ_0	-22.6542	0.1721
	b	0.70526	0.00533
	α	-0.26636	0.00301
	G_m	0.05141	0.00022
	γ	0.06052	0.00109
CDW	G_c	0.05911	0.00245
	T_{CDW}	98.245	0.06283
	Γ_c	8.3818	0.1528

$a_{m0} - \alpha H^2)/b$. This condition indicates that the softening of the magnetic mode reduces its excitation energy toward the acoustic phonon energy, thereby maximizing magnetoelastic hybridization. As the magnetic field increases, the αH^2 term shifts the magnetic energy scale upward, resulting in a displacement of the dip to higher temperatures.

Scaling Analysis. While the multivariable analysis decomposes the ultrasound velocity anomalies into magnetic and CDW contributions it does not by itself demonstrate that these components follow universal fluctuation forms. By rescaling the susceptibilities using their natural energy scales - $\Gamma(T, H)$ for the magnetic channel and Γ_c for the CDW channel - we show that the data collapse onto Lorentzian scaling functions, Fig. 3 (a). Such a collapse would indicate that the extracted parameters correspond to intrinsic fluctuation energy scales of the system. In the scaling analysis we neglect the smooth background contribution eq. (7), modeled as a second-order polynomial in T which represents analytic, non-critical lattice effects that are field independent. Since it does not contain intrinsic fluctuation energy scales, it does not participate in scaling behavior. Scaling is expected only for contributions governed by critical or near-critical fluctuations, where the response depends on dimensionless ratios of relevant energy scales. The magnetic contribution to the velocity shift has the form:

$$\chi_m(T, H) = \frac{G_m}{\delta(T, H)^2 + \Gamma(T, H)^2} = \frac{G_m}{\Gamma(T, H)^2} f_m(x_m),$$

with $\delta(T, H) = \delta_0 + bT + \alpha H^2$ and $\Gamma(T, H) = \Gamma_0 + \gamma H^2$. Factoring out the damping scale, introduces the dimensionless scaling variable and a corresponding Lorentzian function:

$$x_m = \frac{\delta(T, H)}{\Gamma(T, H)}, \quad f_m(x_m) = \frac{1}{1 + x_m^2}. \quad (12)$$

After rescaling by the field-dependent amplitude $G_m/\Gamma(T, H)^2$, all magnetic data collapse onto a single

Lorentzian curve (see the inset of Fig. 3(a)). Similarly, the CDW contribution is described by

$$\chi_c(T) = \frac{G_c}{(T - T_{\text{CDW}})^2 + \Gamma_c^2} = \frac{G_c}{\Gamma_c^2} f_c(x_c), \quad (13)$$

where

$$x_c = \frac{T - T_{\text{CDW}}}{\Gamma_c}, \quad f_c(x_c) = \frac{1}{1 + x_c^2}. \quad (14)$$

Here, Γ_c sets the characteristic fluctuation energy scale. The observed collapse confirms that the CDW response depends only on the reduced distance from T_{CDW} . The successful scaling of both channels [Fig. 3 (a)] demonstrates that the fitted parameters correspond to intrinsic fluctuation energy scales rather than empirical fitting coefficients. The separate Lorentzian form indicate that magnetic and CDW fluctuations coexist over the same temperature range but retain distinct intrinsic fluctuation scales. The peak amplitudes of the scaling functions are given by: $\chi_c^{\text{max}} = G_c/\Gamma_c^2$ and $\chi_m^{\text{max}} = G_m/\Gamma^2$. From our numerical analysis we find $\chi_c^{\text{max}} \gg \chi_m^{\text{max}}$, suggesting either a larger correlation length or a stronger coupling of the CDW order parameter to lattice strain. Within an Ornstein–Zernike framework, where $\chi \sim \xi^2$, the larger CDW amplitude is consistent with more extended CDW correlations and/or stronger coupling to the elastic degrees of freedom.

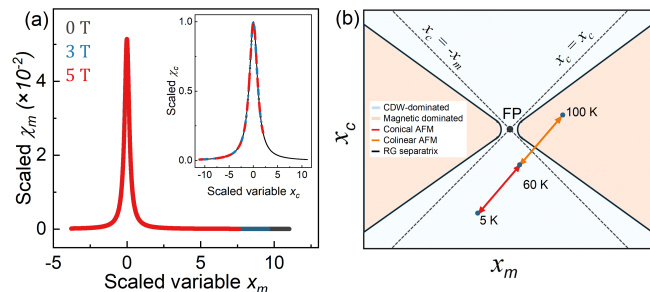


FIG. 3. Representative scaling collapse of (a) magnetic [eq. (8)], and (inset) CDW [eq. (13)] channels. (b) Schematic two-parameter scaling space spanned by (x_m, x_c) , illustrating independent relevant directions associated with magnetic and CDW fluctuations.

In order to understand how effective coupling between phases (magnetic, CDW) changes we apply the renormalization group (RG) technique [27], in which the coexistence of these modes is an input at the level of degrees of freedom and possible fixed points (FP) are outcomes of the RG flow (see also Appendix D). Thus, the full scaling form for the velocity shift can be written as

$$\frac{\Delta v}{v} - \left(\frac{\Delta v}{v} \right)_{\text{bg}} = -\frac{1}{\Gamma^2} \frac{1}{1 + x_m^2} - \frac{1}{\Gamma_c^2} \frac{1}{1 + x_c^2}$$

Each scaling variable x_m and x_c define independent relevant directions associated with magnetic and CDW instabilities. The fixed point where the scaling flow stops

is located at $(0,0)$ being a Gaussian bicritical point. The diagram seen in Fig. 3 (b) shows the linear RG eigen-directions ($x_{\pm} = x_m \pm x_c$, see appendix D) i.e. the diagonals, dominant/second-dominant eigen-direction as special limit of $\Gamma = \Gamma_c$. The scaling variable $x_m = \delta/\Gamma$ represents the ratio between the static magnetic stiffness scale and the dynamical broadening. Moving along x_m corresponds to tuning through the magnetic instability (e.g., cone opening or closing), whereas moving along x_c corresponds to tuning through the CDW instability. When $x_m \rightarrow 0$, the system becomes soft relative to its damping scale, which leads to the observed scaling collapse. The crossover lines seen in Fig. 3 (b) results from the equation: $x_m^2 = 2.5x_c^2 + 1.5$ with $\Gamma_c^2/\Gamma_0^2 \approx 2.5$. As Γ_c/Γ_0 is larger than 1, the CDW fluctuations are dynamically broader, the magnetic mode is sharper and the magnetic dominance region is smaller near origin. The CDW dominance region extends further out. As field is increases $\Gamma_0 + \gamma H^2$ the ration decreases, the hyperbola moves continuously with field and the trajectory bends. Applying a field along c slightly enhances mixing between magnetic and CDW contributions. Dashed lines represents $\Delta v/v$ trajectories (temperature sweep) with arrows indicating the RG “flow direction” from low to high T. At low T trajectories evolve near x_m axis (mostly magnetic), while at high T, trajectories bend toward x_+ due to weak coupling g . Arrows clearly show flows moving away from the fixed point in scaling space as the RG scale increases. To conclude our elementary RG-analysis, the results explains horizontal shifts in $\Delta v/v$ collapse when approaching CDW region and demonstrates that FeGe resides in a mixed regime where both x_m and x_c are finite.

The double-cone magnetic structure was characterized by neutron diffraction [2, 15] and can be parametrized in terms of the total ordered moment amplitude $S^2 = S_{\parallel}^2 + S_{\perp}^2$ and the cone half-angle $\theta = \tan^{-1}(S_{\perp}/S_{\parallel})$. For $\theta = 0$, the system reduces to the collinear AFM state, while $\theta > 0$ corresponds to the conical phase. Decreasing the temperature the cone opens, the transverse component S_{\perp} increases and the interlayer pitch q is nearly constant. To assess how close the system is to an instability or whether the magnetic mode is soft, we use a simplified Landau free-energy density for the magnetic order parameter amplitude S which may be written as:

$$F = \frac{1}{2}\delta(T, H)S^2 + \frac{u}{4}S^4, \quad (15)$$

where $\delta(T, H)$ controls the stiffness (energy cost) of the fluctuations of the order parameter S . The coefficient u multiplies the quartic term S^4 and ensures stability of the ordered state setting the scale of the order parameter amplitude. Free energy minimization yields

$$S^2(T, H) = -\frac{\delta(T, H)}{u} \quad (\delta < 0)$$

Thus, the scaling parameter $\delta(T, H) = \delta_0 + bT + \alpha H^2$ extracted from ultrasound directly controls the square of the ordered moment amplitude. From the global fit for

$T \leq 115$ K, the parameters are obtained as $\delta_0 = -22.65$, $b = 0.705$ K $^{-1}$, and $\alpha = -0.266$ T $^{-2}$ (see Table I). The condition $\delta(T, H) = 0$, which defines the temperature at which the magnetic amplitude softens, reads:

$$T_c(H) = -\frac{\delta_0}{b} - \frac{\alpha}{b} H^2 \approx 32.1 \text{ K} + 0.38 H^2, \quad (16)$$

and is consistent with the experimentally observed minima in the temperature dependence of the characteristic $\Delta v/v$ under applied magnetic field.

Neutron diffraction [2, 15] measures the intensity of magnetic satellites associated with the transverse component. From the minimization criteria, the leading temperature and field dependence up to smooth geometric factors from field-induced changes of the cone angle is:

$$I_{\text{sat}}(T, H) \propto S_{\perp}^2 = S^2 \sin^2 \theta \propto -\delta(T, H), \quad (17)$$

Using the fitted form of $\delta(T, H)$, eq. (17) predicts a linear temperature dependence of I_{sat} at fixed field, and quadratic suppression with magnetic field at fixed temperature. The coefficient $\alpha (= -0.266$ T $^{-2}$) extracted from ultrasound directly quantifies the field sensitivity of the magnetic stiffness controlling the cone angle. Note that the term αH^2 in $\delta(T, H)$ reflects the symmetry-allowed quadratic coupling of the magnetic amplitude to a field applied along the c -axis. In the conical state, such a field modifies both (S_{\parallel} , S_{\perp}) i.e., it changes the cone angle. Because the ordered moment amplitude satisfies $S^2 \propto -\delta$, the quadratic field dependence implies that the field effectively renormalizes the stiffness of the conical state. The scaling collapse of $\Delta v/v$ therefore indicates that the magnetoelastic anomaly is governed primarily by the amplitude of the ordered moment rather than by independent longitudinal and transverse fluctuations.

We conclude finally that ultrasound probes the effective magnetic stiffness dynamically through magnetoelastic coupling, while neutron diffraction measures its static manifestation in the cone amplitude. The observed scaling collapse of $\Delta v/v$ thus supports a unified description in which the temperature and field evolution of the conical state are governed by a single exchange-renormalized stiffness parameter $\delta(T, H)$.

Conclusion and outlook. Our minimal microscopic model of coupled modes quantitatively describes both the temperature and magnetic-field dependence of the low-temperature anomaly and the presence of a robust CDW-related shoulder. The low- T anomaly is naturally explained by phonon–magnon hybridization. Its field dependence enters through a field-dependent magnetic stiffness (αH^2) and field-induced damping broadening (γH^2), reflecting the longitudinal response and distortion of the conical spin structure under $H \parallel c$. The CDW shoulder remains essentially field independent in the measured range, consistent with its predominantly electronic origin and weak magnetic coupling.

Beyond providing an accurate global fit, the extracted parameters reveal an internal scaling structure: the mag-

netic contribution collapses when expressed in terms of the reduced variable $x_m = \delta(T, H)/\Gamma(T, H)$, while the CDW channel scales with $x_c = (T - T_{\text{CDW}})/\Gamma_c$. The combined data can be interpreted within a two-parameter scaling framework in which $\Delta v/v$ is governed by two relevant directions corresponding to magnetic and CDW fluctuations. In this sense, the elastic anomaly behaves analogously to a renormalized susceptibility near coupled instabilities, with the fitted coefficients directly defining the effective stiffness and damping scales of the underlying collective modes.

Essentially, the magnetic scaling variable can be related to the cone angle of the exchange-driven double-cone structure determined by neutron diffraction. In centrosymmetric $P6/mmm$ symmetry, Dzyaloshinskii–Moriya interaction is forbidden, and the conical state arises from frustrated exchange. The scaling of $\Delta v/v$ therefore reflects the renormalization of an exchange-controlled magnetic stiffness rather than a chiral twisting mechanism. Since the neutron satellite intensity is proportional to the square of the transverse spiral component, and hence to the cone angle, the ultrasound softening directly tracks the evolution of the same transverse magnetic amplitude that produces the elastic Bragg satellites. This establishes a quantitative bridge between elastic and neutron probes: ultrasound measures the renormalized susceptibility of the same exchange-driven mode whose static amplitude is detected in diffraction.

The scaling behavior further suggests that the magnetic and CDW channels are only weakly coupled in the investigated field range, with small but measurable cross-coupling that bends the scaling trajectories in the (x_m, x_c) plane. This weak mixing explains why the CDW shoulder remains largely field independent while the magnetic dip shifts systematically with field. In this sense, FeGe provides an experimentally clean realization of a two-channel magnetoelastic problem in which collective modes coexist but remain only moderately hybridized.

In summary, we have demonstrated that ultrasound velocity anomalies in FeGe can be understood within a unified magnetoelastic framework that connects phonon–magnon hybridization, CDW amplitude fluctuations, scaling behavior, and neutron-scattering signatures of the exchange-driven conical state. The results highlight the power of elastic probes to access renormalized collective modes and provide a pathway toward integrating thermodynamic, spectroscopic, and elastic measurements into a coherent description of correlated quantum materials.

ACKNOWLEDGMENTS

We acknowledge support of the HLD at HZDR, member of the European Magnetic Field Laboratory (EMFL). This work was supported by the Deutsche Forschungsgemeinschaft (DFG, German Research Foundation) - TRR 360 - 492547816.

- [1] K Carrander, H Schwartz, and O Beckman, “Magnetic phase diagram of hexagonal fege,” *Physica Scripta* **2**, 313–315 (1970).
- [2] J Bernhard, B Lebech, and O Beckman, “Magnetic phase diagram of hexagonal fege determined by neutron diffraction,” *Journal of Physics F: Metal Physics* **18**, 539–552 (1988).
- [3] Xiaokun Teng, Lebing Chen, Feng Ye, Elliott Rosenberg, Zhaoyu Liu, Jia-Xin Yin, Yu-Xiao Jiang, Ji Seop Oh, M. Zahid Hasan, Kelly J. Neubauer, Bin Gao, Yaofeng Xie, Makoto Hashimoto, Donghui Lu, Chris Jozwiak, Aaron Bostwick, Eli Rotenberg, Robert J. Birgeneau, Jiun-Haw Chu, Ming Yi, and Pengcheng Dai, “Discovery of charge density wave in a kagome lattice antiferromagnet,” *Nature* **609**, 490–495 (2022).
- [4] Taishi Chen, Susumu Minami, Akito Sakai, Yangming Wang, Zili Feng, Takuya Nomoto, Motoaki Hirayama, Rieko Ishii, Takashi Koretsune, Ryotaro Arita, and Satoru Nakatsuji, “Large anomalous Nernst effect and nodal plane in an iron-based kagome ferromagnet,” *Sci. Adv.* **8** (2022), 10.1126/sciadv.abk1480.
- [5] Mason L. Klemm, Tingjun Zhang, Barry L. Winn, Fankang Li, Feng Ye, Masaaki Matsuda, Avishek Maity, Sijie Xu, Xiaokun Teng, Yoshihiko Umemoto, Bin Gao, Ming Yi, and Pengcheng Dai, “Interacting spin and charge density waves in the kagome metal fege,” *Physical Review B* **112** (2025), 10.1103/d88l-4wq8.
- [6] D. Subires, A. Kar, A. Korshunov, C. A. Fuller, Yi Jiang, H. Hu, D. Călugăru, C. McMonagle, C. Yi, S. Roychowdhury, W. Schnelle, C. Shekhar, J. Stremper, A. Jana, I. Vobornik, J. Dai, M. Tallarida, D. Chernyshov, A. Bosak, C. Felser, B. Andrei Bernevig, and S. Blanco-Canosa, “Frustrated charge density wave and quasi-long-range bond-orientational order in the magnetic kagome fege,” *Nature Communications* **16** (2025), 10.1038/s41467-025-58725-2.
- [7] Chenfei Shi, Wenchang Hou, Hanbin Deng, Bikash Patra, Surya Rohith Kotla, Yi Liu, Sitaram Ramakrishnan, Claudio Eisele, Harshit Agarwal, Leila Noohinejad, Ji-Yong Liu, Tianyu Yang, Guowei Liu, Bishal Baran Maity, Qi Wang, Zhaodi Lin, Baojuan Kang, Wanting Yang, Yongchang Li, Zhihua Yang, Yuxiang Chen, Xiang Li, Yuke Li, Yanpeng Qi, Arumugam Thamizhavel, Wei Ren, Guang-Han Cao, Jia-Xin Yin, Bahadur Singh, Xuerong Liu, Sander van Smaalen, Shixun Cao, and Jin-Ke Bao, “Charge density wave with suppressed long-range structural modulation in canted antiferromagnetic kagome FeGe,” *Communications Physics* **8** (2025), 10.1038/s42005-025-02316-6.
- [8] Xiaokun Teng, Ji Seop Oh, Hengxin Tan, Lebing Chen, Jianwei Huang, Bin Gao, Jia-Xin Yin, Jiun-Haw Chu, Makoto Hashimoto, Donghui Lu, Chris Jozwiak, Aaron Bostwick, Eli Rotenberg, Garrett E. Granroth, Binghai Yan, Robert J. Birgeneau, Pengcheng Dai, and Ming Yi, “Magnetism and charge density wave order in kagome fege,” *Nature Physics* **19**, 814–822 (2023).
- [9] Shangfei Wu, Mason L. Klemm, Jay Shah, Ethan T. Ritz, Chunruo Duan, Xiaokun Teng, Bin Gao, Feng Ye, Masaaki Matsuda, Fankang Li, Xianghan Xu, Ming Yi, Turan Birol, Pengcheng Dai, and Girsh Blumberg, “Symmetry Breaking and Ascending in the Magnetic Kagome Metal FeGe,” *Physical Review X* **14**, 011043 (2024).
- [10] Ziyuan Chen, Xueliang Wu, Shiming Zhou, Jiakang Zhang, Ruotong Yin, Yuanji Li, Mingzhe Li, Jishuo Gong, Mingquan He, Yisheng Chai, Xiaoyuan Zhou, Yilin Wang, Aifeng Wang, Ya-Jun Yan, and Dong-Lai Feng, “Discovery of a long-ranged charge order with 1/4 Ge1-dimerization in an antiferromagnetic Kagome metal,” *Nature Communications* **15** (2024), 10.1038/s41467-024-50661-x.
- [11] Hanjing Zhou, Songsong Yan, Dongze Fan, Di Wang, and Xiangang Wan, “Magnetic interactions and possible structural distortion in kagome FeGe from first-principles calculations and symmetry analysis,” *Physical Review B* **108**, 035138 (2023).
- [12] Pietro M. Bonetti, Yi Jiang, Haoyu Hu, Dumitru Călugăru, Michael M. Scherer, B. Andrei Bernevig, and Laura Classen, “Competing phases in kagome magnet FeGe from functional renormalization,” (2024).
- [13] Yilin Wang, “Enhanced spin-polarization via partial g-dimerization as the driving force of the charge density wave in fege,” *Physical Review Materials* **7**, 104006 (2023).
- [14] Shulun Han, Linyang Li, Chi Sin Tang, Qi Wang, Lingfeng Zhang, Caozheng Diao, Mingwen Zhao, Shuo Sun, Lijun Tian, Mark B. H. Breese, Chuanbing Cai, Milorad V. Milošević, Yanpeng Qi, Andrew T. S. Wee, and Xinmao Yin, “Orbital hybridization and magnetic moment enhancement driven by charge density waves in kagome fege,” *Applied Physics Reviews* **12** (2025), 10.1063/5.0260257.
- [15] J Bernhard, B Lebech, and O Beckman, “Neutron diffraction studies of the low-temperature magnetic structure of hexagonal fege,” *Journal of Physics F: Metal Physics* **14**, 2379–2393 (1984).
- [16] Olof Beckman, Lorna J. Sundström, Kjell Carrander, and Leif Lundgren, “Localized versus itinerant electrons in hexagonal fege,” *Solid State Communications* **12**, 1061–1065 (1973).
- [17] Lebing Chen, Xiaokun Teng, Hengxin Tan, Barry L. Winn, Garrett E. Granroth, Feng Ye, D. H. Yu, R. A. Mole, Bin Gao, Binghai Yan, Ming Yi, and Pengcheng Dai, “Competing itinerant and local spin interactions in kagome metal FeGe,” *Nature Communications* **15** (2024), 10.1038/s41467-023-44190-2.
- [18] Xiaokun Teng, David W. Tam, Lebing Chen, Hengxin Tan, Yaofeng Xie, Bin Gao, Garrett E. Granroth, Alexandre Ivanov, Philippe Bourges, Binghai Yan, Ming Yi, and Pengcheng Dai, “Spin-Charge-Lattice Coupling across the Charge Density Wave Transition in a Kagome Lattice Antiferromagnet,” *Physical Review Letters* **133**, 046502 (2024).
- [19] A. Hauspurg, S. Zherlitsyn, T. Helm, V. Felea, J. Wosnitza, V. Tsurkan, K.-Y. Choi, S.-H. Do, Mengxing Ye, Wolfram Brenig, and Natalia B. Perkins, “Fractionalized excitations probed by ultrasound,” *Physical Review B* **109**, 144415 (2024).
- [20] B. Lüthi, *Physical Acoustics in the Solid State* (Springer, Berlin, Heidelberg, 2007).
- [21] S. Zherlitsyn, S. Yasin, J. Wosnitza, A. A. Zvyagin, A. V. Andreev, and V. Tsurkan, “Spin-lattice effects in se-

lected antiferromagnetic materials (review article),” *Low Temperature Physics* **40**, 123–133 (2014).

- [22] J. Sourd, Y. Skourski, L. Prodan, V. Tsurkan, A. Miyata, J. Wosnitza, and S. Zherlitsyn, “Magnon-phonon interactions in the spinel compound mncs_2se_4 ,” *Physical Review B* **110**, 094414 (2024).
- [23] Vladimir Tsurkan, Sergei Zherlitsyn, Lilian Prodan, Viorel Felea, Pham Thanh Cong, Yurii Skourski, Zhe Wang, Joachim Deisenhofer, Hans-Albrecht Krug von Nidda, Joachim Wosnitza, and Alois Loidl, “Ultra-robust high-field magnetization plateau and supersolidity in bond-frustrated mncr_2s_4 ,” *Science Advances* **3** (2017), 10.1126/sciadv.1601982.
- [24] P. B. Littlewood and C. M. Varma, “Amplitude collective modes in superconductors and their coupling to charge-density waves,” *Phys. Rev. B* **26**, 4883–4893 (1982).
- [25] Jan Berges, Nina Giroto, Tim Wehling, Nicola Marzari, and Samuel Ponc e, “Phonon self-energy corrections: To screen, or not to screen,” *Phys. Rev. X* **13**, 041009 (2023).
- [26] Gerald D Mahan, *Many-particle physics* (Springer Science & Business Media, 2013).
- [27] John Cardy, *Scaling and renormalization in statistical physics*, Vol. 5 (Cambridge university press, 1996).

Appendix A: Relation between elastic constants and the renormalized phonon self-energy

To derive a microscopic description of ultrasound velocity anomalies in a multi-component system such as FeGe — involving acoustic phonons, longitudinal and transverse magnons, and CDW fluctuations — we employ a Green’s-function propagator formalism. Within this framework, phononic, magnonic, and CDW degrees of freedom are treated as coupled bosonic fields, and their interactions are described through retarded Green’s functions that capture the dynamical response of the system.

For a bare longitudinal acoustic phonon the dispersion reads

$$\omega_{\mathbf{q}}^{(0)} = v_0 q, \quad (\text{A1})$$

with bare sound velocity v_0 . The corresponding retarded phonon Green’s function is

$$D_0(\mathbf{q}, \omega) = \frac{2\omega_{\mathbf{q}}^{(0)}}{(\omega + i\eta)^2 - (\omega_{\mathbf{q}}^{(0)})^2}. \quad (\text{A2})$$

When phonons couple to magnons and CDW fluctuations, the propagator becomes renormalized. The physical phonon frequencies follow from the poles of the dressed propagator,

$$\omega^2 - (\omega_{\mathbf{q}}^{(0)})^2 - \Pi^{\text{ph}}(\mathbf{q}, \omega) = 0, \quad (\text{A3})$$

where $\Pi^{\text{ph}}(\mathbf{q}, \omega)$ denotes the effective phonon self-energy arising from magnonic and CDW channels.

Assuming weak coupling, $\omega_{\mathbf{q}} \approx \omega_{\mathbf{q}}^{(0)} + \delta\omega_{\mathbf{q}}$, and ex-

panding to leading order yields

$$\delta\omega_{\mathbf{q}} = \frac{\Pi^{\text{ph}}(\mathbf{q}, \omega_{\mathbf{q}}^{(0)})}{2\omega_{\mathbf{q}}^{(0)}} = \frac{\Re\Pi^{\text{ph}}(\mathbf{q}, \omega_{\mathbf{q}}^{(0)})}{2\omega_{\mathbf{q}}^{(0)}} + i \frac{\Im\Pi^{\text{ph}}(\mathbf{q}, \omega_{\mathbf{q}}^{(0)})}{2\omega_{\mathbf{q}}^{(0)}}. \quad (\text{A4})$$

The real part describes the frequency shift (sound-velocity renormalization), while the imaginary part determines the damping and ultrasound attenuation.

Using the acoustic dispersion $\omega_{\mathbf{q}} = vq$, the relative velocity change becomes

$$\begin{aligned} \frac{\Delta v}{v} &= \frac{\Re\Pi^{\text{ph}}(\mathbf{q}, \omega_{\mathbf{q}}^{(0)})}{2(\omega_{\mathbf{q}}^{(0)})^2} \\ &= \frac{1}{2C_0} \Re\Pi^{\text{ph}}(\mathbf{q} \rightarrow 0, \omega \rightarrow 0), \end{aligned} \quad (\text{A5})$$

where $C_0 = \rho v_0^2$ is the bare elastic constant. In this long-wavelength limit ($\mathbf{q} \rightarrow 0$) ultrasound probes the quasi-static elastic response.

The imaginary part of the self-energy governs sound absorption,

$$\alpha \propto \frac{\Im\Pi^{\text{ph}}(\mathbf{q}, \omega_{\mathbf{q}}^{(0)})}{2\omega_{\mathbf{q}}^{(0)}}. \quad (\text{A6})$$

Thus, all microscopic information enters through the renormalized phonon self-energy Π^{ph} .

Appendix B: Gaussian Ginzburg-Landau free energy functionals

We consider in the followings the renormalization of an acoustic phonon mode due to its coupling to magnetic and charge-density-wave (CDW) fluctuations. Within a Gaussian Landau–Ginzburg framework, the free-energy functional in momentum–frequency space reads

$$F = F_{\text{ph}} + F_{\text{mag}} + F_{\text{CDW}} + F_{\text{int}}. \quad (\text{B1})$$

The bare acoustic mode is described by

$$F_{\text{ph}} = \frac{1}{2} \sum_{q, \omega} u(-q, -\omega) D_0^{-1}(q, \omega) u(q, \omega), \quad (\text{B2})$$

with inverse propagator $D_0^{-1}(q, \omega) = \rho\omega^2 - C_0 q^2$, where ρ is the mass density and C_0 the bare elastic constant. Magnetic and CDW fluctuations are treated at Gaussian level,

$$F_{\text{mag}} = \frac{1}{2} \sum_{q, \omega} M(-q, -\omega) \chi_m^{-1}(q, \omega) M(q, \omega), \quad (\text{B3})$$

$$F_{\text{CDW}} = \frac{1}{2} \sum_{q, \omega} \psi(-q, -\omega) \chi_c^{-1}(q, \omega) \psi(q, \omega), \quad (\text{B4})$$

where $\chi_m(q, \omega)$ and $\chi_c(q, \omega)$ denote the dynamical magnetic and CDW susceptibilities, respectively. We assume

bilinear coupling between strain and the collective modes,

$$F_{\text{int}} = -g_m \sum_{q,\omega} u(-q, -\omega) M(q, \omega) - g_c \sum_{q,\omega} u(-q, -\omega) \psi(q, \omega). \quad (\text{B5})$$

Since the functional is quadratic in M and ψ , these fields can be integrated out exactly. The resulting effective free energy for the phonon field becomes

$$F_{\text{eff}} = \frac{1}{2} \sum_{q,\omega} u(-q, -\omega) [D_0^{-1}(q, \omega) - \Pi^{\text{ph}}(q, \omega)] u(q, \omega), \quad (\text{B6})$$

with phonon self-energy

$$\Pi^{\text{ph}}(q, \omega) = g_m^2 \chi_m(q, \omega) + g_c^2 \chi_c(q, \omega). \quad (\text{B7})$$

In the long-wavelength limit, the relative change of the sound velocity is determined by the real part of the static self-energy as seen in (A5). No further theoretical steps will be taken instead one attempts to formulate useful phenomenological susceptibilities to fit the experimental data.

Appendix C: RPA susceptibilities

Examples shown here are text-book[26] computations of standard random-phase approximation (RPA) susceptibilities.

Charge-Density-Wave Susceptibility

The CDW susceptibility is defined as the density-density correlation function

$$\chi_c(q, i\Omega_n) = \int_0^\beta d\tau e^{i\Omega_n \tau} \langle T_\tau \rho_q(\tau) \rho_{-q}(0) \rangle. \quad (\text{C1})$$

For an itinerant electron system, the bare susceptibility is given by the particle-hole bubble,

$$\chi_{0,c}(q, i\Omega_n) = -T \sum_{k, i\omega_m} G(k, i\omega_m) G(k+q, i\omega_m + i\Omega_n). \quad (\text{C2})$$

After performing the Matsubara frequency summation one obtains the Lindhard form

$$\chi_{0,c}(q, i\Omega_n) = \sum_k \frac{f(\xi_{k+q}) - f(\xi_k)}{i\Omega_n - (\xi_{k+q} - \xi_k)}. \quad (\text{C3})$$

Within the RPA, the CDW susceptibility becomes

$$\chi_c^{\text{RPA}}(q, i\Omega_n) = \frac{\chi_{0,c}(q, i\Omega_n)}{1 - V_q \chi_{0,c}(q, i\Omega_n)} \quad (\text{C4})$$

where V_q is the effective interaction in the charge channel. Near a second-order CDW instability at wave vector Q , the denominator may be expanded as

$$1 - V_Q \chi_{0,c}(q, i\Omega_n) \simeq a_c(T) + c_c(q - Q)^2 + \gamma_c |\Omega_n|. \quad (\text{C5})$$

Thus, close to the transition,

$$\chi_c^{\text{RPA}}(q, i\Omega_n) = \frac{1}{a_c(T) + c_c(q - Q)^2 + \gamma_c |\Omega_n|} \quad (\text{C6})$$

with $a_c(T) \propto T - T_{\text{CDW}}$. In the static limit this reduces to a Lorentzian form, justifying its use in fitting procedures.

2. Transverse Magnetic Susceptibility

The transverse spin susceptibility is defined as

$$\chi_T(q, i\Omega_n) = \int_0^\beta d\tau e^{i\Omega_n \tau} \langle T_\tau S_q^+(\tau) S_{-q}^-(0) \rangle. \quad (\text{C7})$$

The bare transverse susceptibility is

$$\chi_{0,T}(q, i\Omega_n) = -T \sum_{k, i\omega_m} G_\uparrow(k, i\omega_m) G_\downarrow(k+q, i\omega_m + i\Omega_n). \quad (\text{C8})$$

After frequency summation,

$$\chi_{0,T}(q, i\Omega_n) = \sum_k \frac{f(\xi_{k+q,\downarrow}) - f(\xi_{k,\uparrow})}{i\Omega_n - (\xi_{k+q,\downarrow} - \xi_{k,\uparrow})}. \quad (\text{C9})$$

Within RPA (Stoner theory),

$$\chi_T^{\text{RPA}}(q, i\Omega_n) = \frac{\chi_{0,T}(q, i\Omega_n)}{1 - I \chi_{0,T}(q, i\Omega_n)} \quad (\text{C10})$$

where I is the exchange interaction. One distinguishes between the paramagnetic and the ordered regime. Near a magnetic instability at Q ,

$$1 - I \chi_{0,T} \simeq a_m(T) + c_m(q - Q)^2 + \gamma_m |\Omega_n|, \quad (\text{C11})$$

yielding the overdamped paramagnon form

$$\chi_T^{\text{RPA}}(q, i\Omega_n) = \frac{1}{a_m(T) + c_m(q - Q)^2 + \gamma_m |\Omega_n|} \quad (\text{C12})$$

with $a_m(T) \propto T - T_N$. Within the ordered phase (below T_N), in the magnetically ordered state, transverse fluctuations become propagating spin waves. The susceptibility develops poles of the form

$$\chi_T^{\text{RPA}}(q, i\Omega_n) = \frac{Z_T}{\Omega_n^2 + \omega_T^2(q, H, T) + \Gamma_T |\Omega_n|} \quad (\text{C13})$$

where $\omega_T(q, H, T)$ is the spin-wave dispersion and Γ_T describes damping.

In the static limit relevant for ultrasound experiments,

$$\chi_T^{\text{RPA}}(0, 0) = \frac{Z_T}{\omega_T^2(0, H, T)}. \quad (\text{C14})$$

For a conical magnetic state in an external field,

$$\omega_T^2(H, T) = \omega_{T_0}^2(T) + \alpha H^2, \quad (\text{C15})$$

leading to

$$\chi_T^{\text{RPA}}(0, 0) = \frac{Z_T}{\omega_{T_0}^2(T) + \alpha H^2}. \quad (\text{C16})$$

Connection to the Phonon Self-Energy: the renormalized phonon self-energy is obtained from

$$\Pi(q, i\Omega_n) = g_m^2 \chi_T^{\text{RPA}}(q, i\Omega_n) + g_c^2 \chi_c^{\text{RPA}}(q, i\Omega_n), \quad (\text{C17})$$

demonstrating that both magnetic and CDW channels enter through their respective RPA susceptibilities on the Matsubara axis.

Appendix D: RG-flow analysis for FeGe

In FeGe there exists a magnetic mode, a CDW mode and we consider a symmetry-allowed coupling g . The renormalization group (RG) analysis answer the question how do these modes influence each other when the scale is changed. The renormalization group trajectories are described by the equations:

$$\begin{aligned} \dot{x}_m &= x_m + gx_c \\ \dot{x}_c &= x_c + gx_m \end{aligned}$$

and are straight lines in eigenbasis. A fix point satisfies: $\dot{x}_m = 0$ and $\dot{x}_c = 0$. In our linear model this occurs at $(x_m, x_c) = (0, 0)$. The origin corresponds to the symmetric, disordered phase. The fix point corresponds to $\delta(T, H) = 0$ and $T = T_{CDW}$, which physically means that the magnetic mode is soft and the CDW mode is critical. The diagonalization of the flow matrix corresponding to the coupled differential equations gives the eigenvectors $v_+ = (1, 1)$ and $v_- = (1, -1)$ and correspond to the in-phase combination ($x_+ = x_m + x_c$ magnetic + CDW) and out-of-phase combination ($x_- = x_m - x_c$ magnetic - CDW). In our linearized weak-coupling flow, the origin is just the Gaussian fixed point. Because the flow is linear and symmetric the only fixed point is the origin. The system flows away along eigen-directions. Thus, we see dominance, not true coexistence.

We can extract an effective weak coupling g_{eff} (entering the flow equations) from the experimental $\Delta v/v$ trajectories by projecting them onto the eigen-directions

of the coupled RG flow. If the experimental trajectory in the (x_m, x_c) plane is exactly along x_+ then it follows the dominant eigen-direction. any deviation measures an effective tilt that can be translated into a g_{eff} . So one is left to compute the slope of the experimental trajectory ($\Delta x_c / \Delta x_m$). The starting point of the experimental trajectory, at high temperatures $T > T_{CDW}$, $x_c > 0$. The x_m is dominated by the term bT in $\delta(T, H)$ and so $x_m > 0$. The trajectory starts in the first quadrant. the starting point is far from criticality at large radial distance: $l = \ln(x_m^2 + x_c^2)/2$

We derive the crossover line in the (x_m, x_c) plane separating magnetic-dominated and CDW-dominated regimes using the scaled variables. The crossover occurs when $\chi_m = \chi_c$ which leads to the following equation:

$$\begin{aligned} x_m^2 &= \frac{\Gamma_c^2}{\Gamma^2} (x_c^2 + 1) - 1 \\ x_m^2 - \frac{\Gamma_c^2}{\Gamma^2} x_c^2 &= \frac{\Gamma_c^2}{\Gamma^2} - 1 \end{aligned}$$

Which represents the equatoin of a hyperbola. when $\Gamma_c^2/\Gamma^2 > 1$ the hyperbola opens along x_m while $\Gamma_c^2/\Gamma^2 < 1$ hyperbola opens along x_c . The special case $\Gamma_c = \Gamma$ reduces to equal scales $|x_m| = |x_c|$ which geometrically represents the diagonal boundaries. The hyperbolas delimit the physical dominance boundaries.

From the fitted values of FeGe, $\Gamma_0 = 5.29$ and $\Gamma_c = 8.38$, and the ration of the two is ≈ 2.5 (numerical value taken from Tab. I). Thus, the crossover equation is:

$$x_m^2 = 2.5x_c^2 + 1.5$$

The CDW fluctuations are dynamically broader, the agnetic mode is sharper and the magnetic dominance region is smaller near origin. The CDW dominance region extends further out. As field is increases $\Gamma_0 + \gamma H^2$ the ration decreases, the hyperbola moves continuously with field and the trajectory bends.

Solving the couples RG-equations we obtain the experimental trajectories that follow almost straight lines with slopes that change with field and with weak g_{eff} -couplings (Fig. 3(b)). This indicate that FeGe sits near a weakly coupled bicritical point.

As you move along RG scale (or temperature) FeGe goes from magnetic-dominated to CDW-dominated mode within the temperature range 60 K (the cone regime) to 100 K (the CDW regime).